Proceedings of the ASME 2022 Heat Transfer Summer Conference
HT2022
July 11-13, 2022, Philadelphia, PA

HT2022-81856

Convective Heat Transfer Potential of Particles/airflow Through Single Cell Thick Additively Manufactured Octet-Shaped Lattice Frame Material

Youssef Aider
Department of Mechanical Engineering
Mississippi State University
Mississippi State, MS USA

Heejin Cho
Department of Mechanical Engineering
Mississippi State University
Mississippi State, MS USA

Prashant Singh
Department of Mechanical Engineering
Mississippi State University
Mississippi State, MS USA

Abstract

Particle-to-Supercritical Carbon Dioxide (sCO_2) heat exchangers are one of the most critical components of the next-generation Concentrating Solar Power (CSP) plants. There have been several efforts to enhance the overall heat exchanger performance which essentially comprises of thermal resistances offered by sCO_2 channel, wall (separating sCO_2 with particles) thickness, particle-wall contact resistance and particle-side effective heat transfer coefficient. This study is focused towards reducing the particle side thermal resistance by incorporating single unit cell thick reticulated Octet lattice frame structures on the falling particle side to enhance the effective thermal conductivity of the particle channel and to enhance convective heat transfer between the falling particles and the solid phase of the falling particle channel (endwalls and fibers). Steady-state experiments were conducted to measure the effective thermal conductivity of lattice frame material for two cases: a) when void space was occupied by air, b) when void space was occupied with particles. Further, convective heat transfer experiments have been conducted with both air (steady-state) and particles (quasi steady-state) as "working fluid" for panels sandwiching the Octet array. Three different lattice porosities ranging from 0.75 to 0.9 have been tested for a wide range of air flow rates and a fixed particle flow rate (highest potential).

1. INTRODUCTION

Concentrating Solar Power (CSP) is a promising technology to meet our next generation of energy needs from a sustainability perspective. However, in recent times, Photovoltaic (PV) technology has witnessed rapid development when compared to CSP, driving the $/kWh to significantly lower levels compared to that of CSP [1]. In addition, the cost of building and maintaining solar concentrating mirrors is still an issue. Despite the cost drawbacks, CSP technology advancement is still imperative as even though currently, the PV technology has lower $/kWh, it still relies on continued presence of direct sunlight and electrical energy storage in batteries at large power scales is expensive and has its own challenges. On the other hand, CSP plants can store energy at a much larger scale by using thermal energy storage (TES) systems [2]. Currently implemented CSP power heat storage is limited to the use of molten salt where existing molten salt power plants can store energy for up to 8 hours after darkness for parabolic trough and 15 hours for central receiver technologies [3]. After that, the salt needs to be heated with conventional methods, such as natural gas, to continue the power production to the next sunlight period and to prevent salt solidification. Furthermore, the operation temperature of molten salt CSP technology is limited to approximately 565ºC due to the limitations imposed by the thermophysical properties of the salt [4].

Replacing salt with solid bulk of particles has been tested by many researchers and has been proven to have the potential for working as a medium for storing solar energy. Particles can also be heated directly with concentrated sunlight to temperatures exceeding 1000ºC [5–7]. This high-temperature operation can achieve much higher efficiency by using Brayton power cycle based on particle-to-sCO_2 [8,9] heat exchangers. Much research done on particle implementation in CSP plants focuses on the receiver side of the power plant [5]. However, the particle-to-sCO_2 heat exchanger aspect of CSP plan has not received a similar attention, and it has been observed that high overall heat transfer coefficient of particle-to-sCO_2 heat exchanger is critical in realizing the benefits offered by particle route in terms of $/kWh. One of the earliest and simplest particles-to-fluid heat exchanger designs relied on the use of tube bundles. The fluid, which is usually steam, is carried inside the tubes while

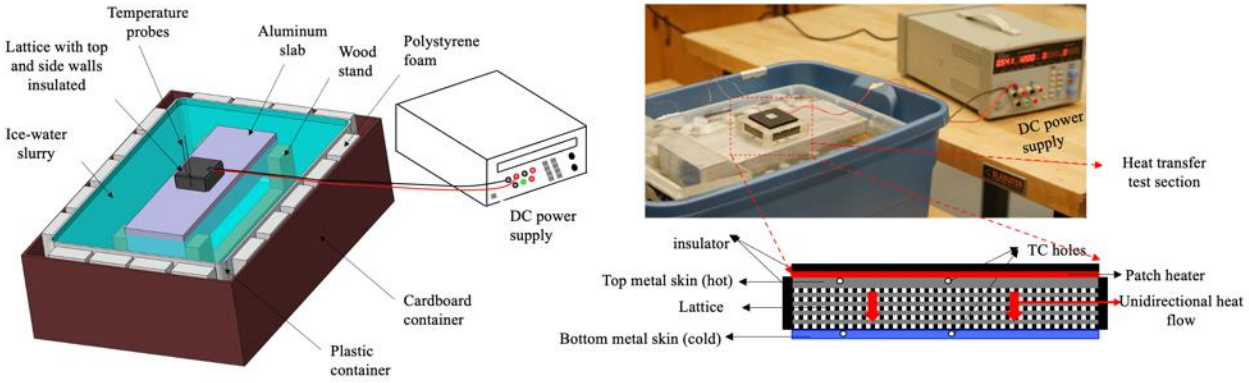

Fig. 1 Schematic of the effective thermal conductivity setup, snapshot of the actual setup and schematic of instrumented lattice sample

a heated bed of solid particles is driven around the tubes with the help of gravity. Studies showed that the heat transfer between the particle bed and a tube is highly localized because of what is known as stagnation and void region located at the top and bottom of the tube, respectively. This challenge led the researchers to develop innovative ways to limit the occurrence of these regions, such as, changing the shape of the tubes from circular to helical [10], relative arrangement of the tubes [11,12], and adding an agitator that influences the flow of particles around the tubes [13], and so on. More efficient heat exchangers such as shell-and-plate and shell-and-tube have also been considered. Albrecht et al. [14] developed and tested a shell-and-plate particle-to-sCO_2 packed bed heat exchanger and achieved a heat transfer coefficient ranging from 50 to 80 W/m^2K at an intermediate temperature of 500 ºC. These heat transfer coefficients are not high enough to realize the particle route's benefits and significant enhancement in this aspect is imperative to meet the $/kWh metrics to prove the technology economically viable.

Theoretical models on a shell-and-plate packed bed heat exchanger showed that with the right combination of the particles size and the distance between the plates, it is possible to achieve an overall heat transfer coefficient approaching 400 W/m^2K at higher temperatures [15]. Research showed that smaller particle size, smaller channel width, and higher particle velocity could enhance the heat transfer coefficient between the hot side (particles) and the cold side (sCO_2). It is also shown that the effective thermal conductivity of the solid particle bed becomes a dominant factor in the heat transfer coefficient at higher particle flow velocity [16]. Recently, a parallel plate particle-to-sCO_2 heat exchanger with microchannels carrying the fluid has been adopted. The channels can be chemically etched into the plates and diffusion bonded [17]. The microchannel parallel plate heat exchanger was experimentally tested at different temperatures ranging from 200ºC to 500ºC achieving a heat transfer coefficient approaching $400W/m^2K$. From these studies, we can see that the parallel palate heat exchanger design achieved the highest reported heat transfer coefficient for packed beds. The studies also showed that reducing the width between the plates, hence decreasing the particle flow channel width, can improve the heat transfer coefficient. This can be attributed to the fact that the reduction in the channel width increased the particle refresh rate at the walls.

In this study, a novel enhanced heat transfer concept is develop for the falling particle channel side of the particle-to-sCO2 heat exchanger, where the convective heat transfer coefficient is enhanced by packing the parallel plates with Octet-shaped lattices. The Octet unit cells and the surrounding plates were additively manufactured in 420 Stainless steel with 40% bronze infiltration via. Binder jetting technology. The Octet lattice has been chosen after carrying out direct simulations which quantified its superior heat transfer enhancement characteristics compared to other unit cell topologies [18]. Following sections present details of different experimental setups employed to measure effective thermal conductivity of lattices made from Octet unit cells where void space is packed with particles of varying diameter, forced convection setup to quantify overall convective heat transfer coefficient of sandwich-type Octet panel with air as working fluid. Finally, a unique test facility was built to carry out particle-based heat transfer experiments. Post this section, the results are presented and analyzed. The paper concludes with major findings from this comprehensive experimental program and path forward based on these findings.

2. EXPERIMENTAL SETUPS AND MEASUREMENT TECHNIQUES

In this part of the study, we are reporting effective thermal conductivity of lattice frame for two cases where a) void space was occupied by air, b) void space was occupied by particles. Further, convective heat transfer capabilities of single cell thick lattice for air and particle flows has been investigated experimentally. To this end, different experimental setups were built to conduct above experiments. Following sub-sections

provides details of the experimental setups, tested configurations, and measurement techniques.

2.1 Effective thermal conductivity setup

The effective thermal conductivity setup is shown in Fig. 1. This experiment was steady-state in nature where a unidirectional heat flow was achieved from top plate to bottom plate of the sample, where Octet-shaped unit cells were sandwiched between the two plates. A cold thermal reservoir was created with the help of an ince-water slurry which was periodically stirred to avoid thermal stratification. An Aluminum slab (10 x 10 x 2.5 cm^3) was then partially submerged into the chilled reservoir which acted as a near-constant cold reservoir, owing to its large thermal mass. The lattice sample was made from a 5 x 5 array of Octet-shaped unit cells in the span and the test sample was one unit cell thick. The Octet unit cell was contained in a Cube of edge length 10 mm. Three samples of design lattice porosities (γ) of 0.75, 0.8 and 0.886 were tested for effective thermal conductivity. The actual porosities of the additively manufactured lattices was 0.712, 0.772, 0.867, respectively. Earlier studies on effective thermal conducitivity of lattices confirm that the porosity has a first order effect for a given solid-fluid pair, hence it is imperative that accurate measurements of porosity be carried out in such experimental investigations. It can be seen that the actual porosities differ from the intended ones (Fig. 2), and the deviation is attributed to AM process – a trend observed in many research efforts across the board. We also carried out in-house CT-scanning of the printed parts to inspect them for defects, roughness etc, and found that at some locations, there were thinner than usual fiber diameters and higher solid mass at the fiber junctions.

Further, the fibers and the endwalls were rough, however, for the effective thermal conductivity experiments carried out on the samples shown in Fig. 2, is not expected to be significantly effected by such local non-uniformities as the air occupying the void space is essentially stagnant and that the net porosity representative of all the inherent defects, roughnesses, deviations from the CAD model, accounts for all of them.

The effective thermal conductivity was determined using Fourier's law of conduction, and its expression is given in Eq. 1. A constant heat flux boundary condition was maintained at the top wall of the sample while the bottom wall was glued firmly with the Aluminum slab which served as the cold reservoir. Steady-state heat transfer experiments were conducted at three different heat flux values, and effective thermal conductivity was determined for each case, to ensure that the determined value was independent of the applied thermal boundary condition. The net heat conducted across the one unit cell thick sample was calculated by subtracting the stray heat loss from the total heat supplied.

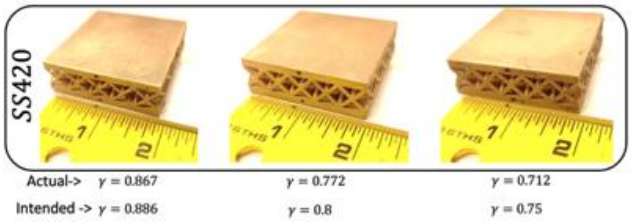

Fig. 2 Three samples of different porosities tested for effective thermal condudcitivty (also indicated are the designed versus actual porosities)

The stray heat loss venues involved the top wall insulation and the four side wall insulations. Thin thermocouples were secured at the inner and outer skins of the insulation to calculate the stray heat loss, with the knowledge of the thermal conductivity of the insulation material (Eq. 2). This accounting of the heat loss ensured that the reported effective thermal conductivity is only a contribution of the unit cell topology, solid- and fluid-phase thermal conductivities, and lattices's effective porosity.

$$k_{eff} = \frac{(q_{cond}/A)\Delta z}{\Delta T} = \frac{(\{q_{total} - \sum q_{loss}\}/A)\Delta z}{\tilde{T}_{top} - \tilde{T}_{bot}} \quad (Eq.\,1)$$

$$\sum q_{loss} = \frac{k_{ins}}{t_{ins}}\left[A\left(T_{Top,in} - T_{Top,out}\right) + 4b\Delta z\left(T_{side,in} - T_{side,out}\right)\right] \quad (Eq.\,2)$$

where, "*A*" is the lattice base area, "Δz" is the thickness of single unit cell of lattice and "*b*" is the edge length of square cross-sectioned lattice.

2.2 Forced convection setup with air as "working fluid"

Figure 3 shows the schematic of the experimental facility used in the present study. Air was the working fluid in this part of the study and was drawn from a compressed air tank maintained at ~ 1MPa. A pressure regulator was placed downstream of the compressor to adjust the mass flow rate to a desired value. The air was then directed to an orifice plate for flow metering. Differential pressure across the orifice meter, static air pressure upstream of the orifice plate and air temperature were measured using Dwyer 477AV-2 (0-10 kPa), Dwyer DPG-002 (0-100 kPa) and fast response T-type thermocouple, respectively, which were then fed into an in-house MATLAB code to determine the mass flow rate. The metered flow was then passed through a control valve regulating the flow into the test section.

The transition of the flow from circular pipe to square duct was executed with the help of a trapezoidal shaped-diffuser.

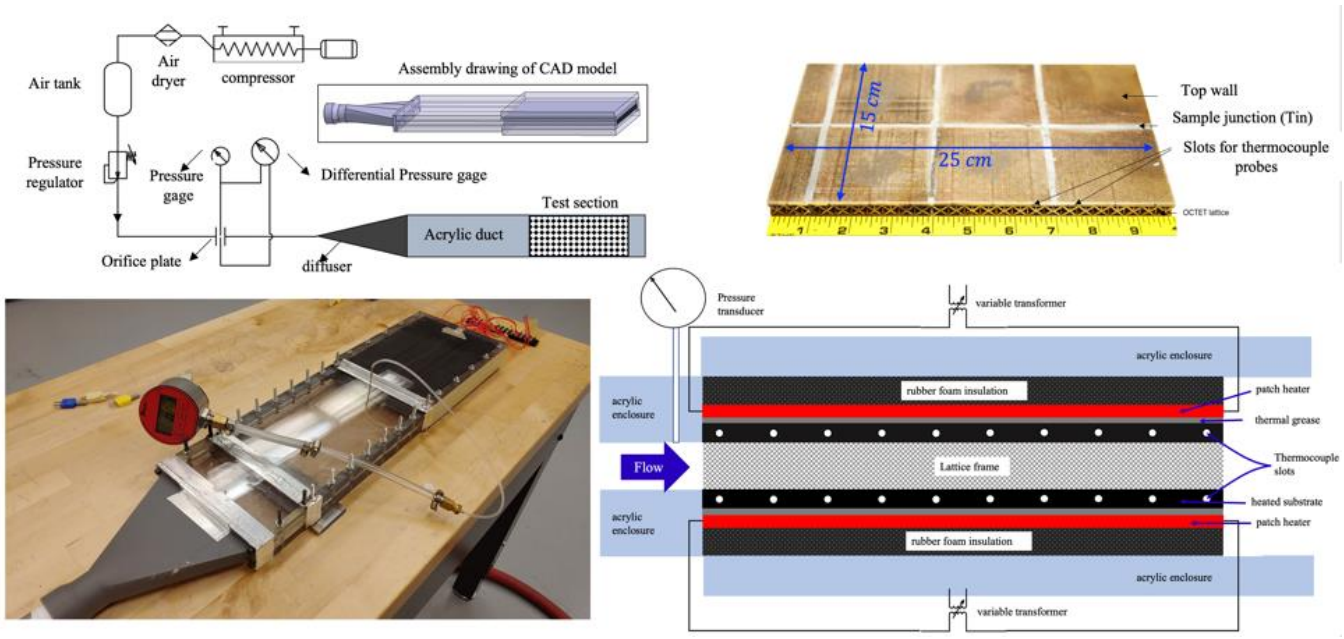

Fig. 3 Assembly drawing of air-based forced convection setup (top left), snapshot of the flow straightening and heat transfer test sections (bottom left), additively manufactured sandwich-type Octet panel (top right), schematic of the instrumentation at the heat transfer test section (bottom right)

The sandwich panel featuring array of Octet unit cells had top and bottom walls of 15 cm x 25 cm dimension and thickness was 10 mm. Hence, the flow channel had high aspect ratio (width/height) of 15. It is generally challenging to achieve a uniform hydrodynamically developed flow at the entrance of the test section with an aspect ratio of 15. To address this, a ~ 33 cm long plexiglass duct was installed between the heat transfer test section and the trapezoidal diffuser. This was done to ensure that the reported heat transfer coefficient in the entry region of the test section does not have a contribution of under-developed nature of the approaching flow.

The samples used in this part were made from reituclating Octet unit cell in span where the sample was one unit cell thick. The sample was additively manufactured from bronze infiltrated stainless steel 420 using binder jetting technology. The bed size of the 3D printer limited the maximum size of the lattice which can be printed in one run. To this end, the sandwich panel show in Fig. 3 was obtained by 3D printing different smaller sections and then joining them together by soldering with Tin metal. Tin metal, with its high thermal conductivity (60W/mK), creates a thermal bridge between the different sections, ensuring excellent thermal contact between them. The assembled heat exchanger had solid walls with multiple thermocouples holes to allow temperature measurement at different locations inside the walls.

Figure 3 (bottom right) also shows the schematic of the heat transfer test section. The sandwich panel was heated with patch heaters attached to both top and bottom walls using thermally conductive silicone compound (CHEMPLEX ® 1381 DE). Rubber foam thermal insulation with thermal conductivity of 0.037 (W/mK) and thickness of 3.175 mm was pasted on the surface of the heaters. The temperature difference across the insulation was measured at different locations in the panel span to measure the heat losses. T-type thermocouples were used to measure the temperature inside each thermocouple slot which was very close to the solid-fluid interface and this temperature was treated as the representative wall temperature in the convective heat transfer coefficient calculations. A constant heat flux type thermal boundary condition was created with the help of the patch heaters mentioned above, where the heating power was controlled with variable transformers with voltage indicators.

The steady-state heat transfer experimental procedure included heating both top and bottom panels via the glued patch heaters and wait for the first steady state. Note that at this stage, the air flow was not switch on. Once the first steady-state was reached, the air flow rate corresponding to a desired channel flow velocity was set through the heated test section, which was then allowed to cool down since the air supply was at nearly at the laboratory ambient temperature (~20℃). Once the second steady was reached (with continuous airflow), the measurements of flow inlet temperature, wall temperature at discrete locations, and temperature drop across the insulation were carried out. Note that the panel was wide (15 cm x 25 cm) and a representative wall temperature would only be found by measuring local wall temperatures at several discrete locations on both the top and bottom walls.

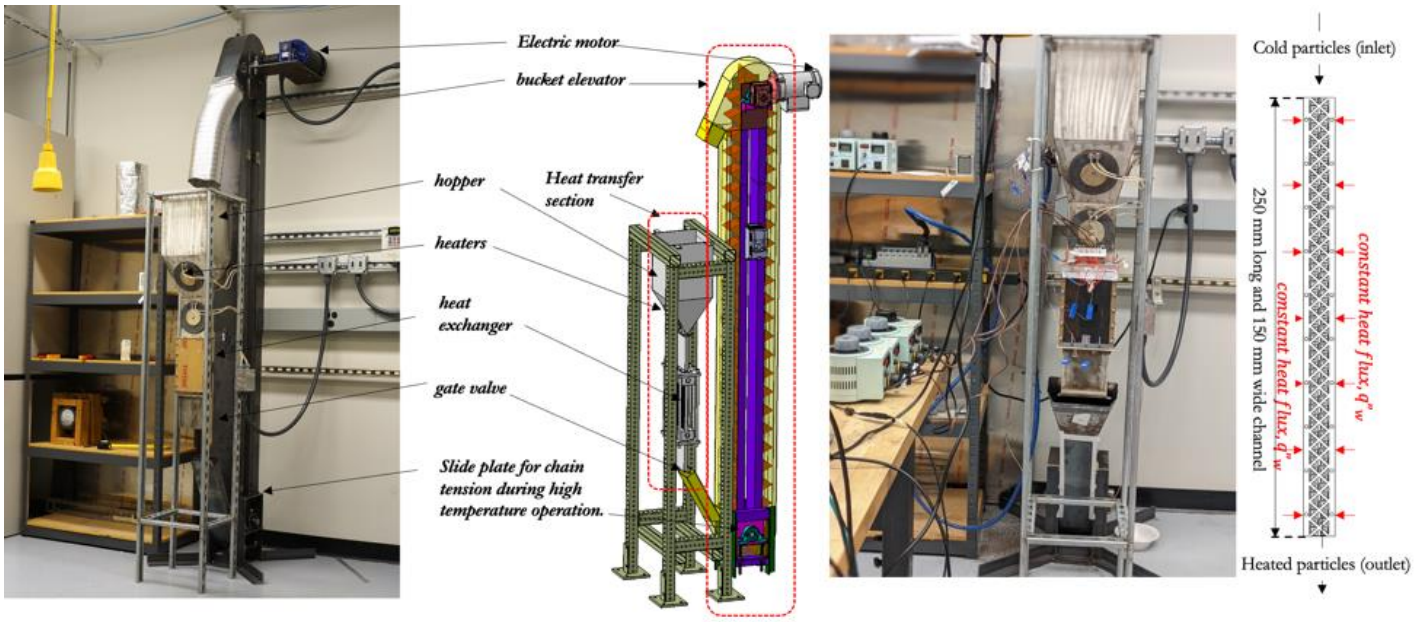

Fig. 4 Particle heat transfer test facility

An array of 10 equi-spaced thermocouple slots was incorporated (in the AM phase itself) at spanwise locations of W/2 and W/6, at both top and bottom walls, where W is the width of the panel. Under the assumption that the temperature distribution would be symmetric about the channel centerline in the streamwise direction, the representative wall temperature at a particular streamwise location was then obtained by calculating the area averaged temperature based on the two measurements carried at the span of W/2 (centerline) and W/6. A trendline for streamwise variation of wall temperature was obtained for both top and bottom walls, to get a continuous variation ($T_w(x)$) from the discrete measurements. Convective heat transfer coefficient at these discrete location along the streamwise direction is given as,

$$h(x) = \frac{q"_{conv}}{T_w(x) - T_f(x)} \quad (Eq.3)$$

where, $q"_{conv} = (q_{total} - q_{loss,insulation})/A$, and local fluid temperature, $T_f(x) = T_{f,in} + \left(q"_{conv} W/\dot{m}c_p\right)x$. The local convective heat transfer coefficient ($h(x)$) obtained from above procedure was then used to calculate a *representative* "h" for each row of unit cells in the streamwise direction.

2.3 Particle heat transfer test facility

The heat transfer test section described in Section 2.2 (Fig. 3, top right) above was used in the experiments for determination of convective heat transfer coefficient with particles as "working fluid". Unlike air-based convection experiments, the particles which carry heat from the test section had to be transported back into the system. To this end, a bucket elevator-system was designed, developed, and built for these experiments. Buckets elevator works by rotating a set of a buckets attached to a chain or a belt, and by doing so, the buckets scoop the particles from the bottom of the elevator casing and discharge at the top. Bucket elevators are more complex to design and manufacture, compared to static screw elevator and drag chain conveyor. However, the benefits of their reliability, smaller footprint, and the ability to work at elevated temperatures outweigh the cost and complexity of the manufacturing process.

The acutal assembled test facility, assembly CAD model, instrumented heat transfer test section, and schematic representation of heat transfer scenario involving falling particles are shown in Fig. 4. Particles are first stored at room temperature in the top hopper while the top and bottom walls of the sandwich panel was being electrically heated with patch heaters. The particles were held until the panel walls reach a temperature of 100ºC. A gate valve was installed right downstream of the heat transfer section, which facilitated the on/off type flow of particle across the test section. Once the desired panel wall temperatures were achieved, the gate valve was flipped and the elevator was started at the same time, to allow the transport of the *spent* particle back into the top hopper via a series of equi-spaced buckets.

It should be noted that particle heat transfer experiments are different from the air-based experiments in the sense that the working fluid was recirculated and fed back into the heat transfer section. Due to convection, particles carry away some heat from the heated walls and the same batch of particles is transported back into the hopper above the test section via the bucket elevator. During the transport in the buckets, the particles do loose some heat to the laboratory ambient,

however, in our initial testing and the design of heat transfer experiments, we observed that the particle temperatures continue to keep increasing as they are recirculated for a prolonged duration. Further, it was decided that bucket-elevator-based experiments should not be allowed to run for very long periods of time, as particles can get destroyed/crushed during the transport, which may inherently change the particle size distribution with time, and a satisfactory steady state could never be achieved, both in the heat transfer sense and the working fluid rhealogical properties sense.

To address above aspect, a novel quasi-steady state heat transfer methodlogy was devised exlusively for this part of the investigation, which could effectively provide local convective heat transfer coefficient where heat transfer was facilitated through falling particles. In this approach, firstly the hopper is filled with desired type of particles where the total mass of particles was decided such that a packed bed flow could be achieved at the heat transfer test section. Once the hopper was charged with particles, the heating process was started where all the eight patch heaters occupying the entire 150 x 250 mm^2 panel on both left and right sides of sandwiched panel were heated. Once the steady-state heat transfer condition was obtained, the particle flow rate through the Octet panel was initiated by opening the gate valve installed at the bottom of the heat exchanger to 100%. Note that this facility also allows a fine control over the particle flow rate through the gate valve while still maintaining a packed moving bed through the Octet panel. In this study, the maximum possible particle mass flow rate was studied, hence 100% opening of the gate valve was set. Prior to the particle flow start, the data acquisition system was initiated which involved over 20 thermocouple measurements across the heat transfer test section, including a pair of temperature measurements for particle inlet and outlet. Once the particles started to flow through the Octet panel, the walls of the panel started to cool down rapidly to a local minima. At that point onwards, the particle and the wall temperatures continued to slowly increase for the remainder of the transient experiment. In the heat transfer coefficient calculation, the wall and particle temperatures during this slow heat ramp up period was taken into consideration and the local convective heat transfer coefficient was determined through the following eqation:

$$h(x,t) = \frac{q''_{conv}(t)}{T_w(x,t) - T_f(x,t)} \quad (Eq.4)$$

where, $q''_{conv}(t)$ is the heat convected away from the walls via the particles in motion and this was obtained by subtracting the local heat losses from the backside of the eight patch heaters occupying and supplying constant heat flux on the left and right sides of the panel. Note that the temperature drop across the insulation material was measured at multiple locations along the streamwise length and also recorded along with the wall temperature at the same fequency throughout the transient operation. The heat loss however was minimal compared to the total heat supplied.

2.3.1 Particle type and size distribution

The particles used in the experiment are made from sintered bauxite. Three different particle batches were tested: CARBOBEAD-CP 40/100 with a mean particle diameter of 266.566 µm, CARBOBEAD-CP 30/60 with a mean particle diameter of 397.132 µm, and CARBOBEAD HSP 20/40 with a mean particle diameter of 966.129 µm. Particle size analysis was performed using Anton Paar PSA 1190 LD particle size analyzer.

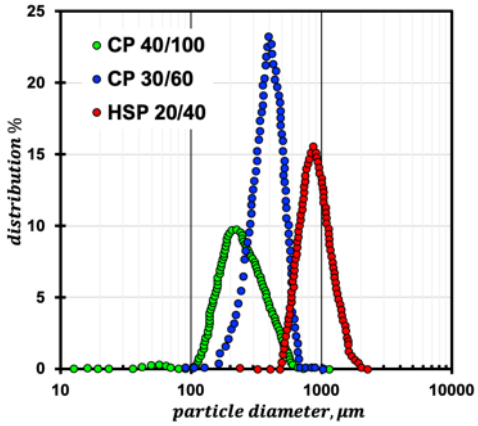

Fig. 5 Particle size distribution

The particle size analysis showed that each particle batch has a normal size distribution and the distribution is shown in Fig. 5.

3. RESULTS AND DISCUSSION

In this section, we are presenting experimental results on effective thermal conductivity, convective heat transfer coefficient for air and particles as working fluids.

3.1 Effective Thermal Conductivity (k_{eff})

Effective thermal conductivity experiments were carried out for three cases, a) packed bed of particles, b) lattice with void space occupied by air, c) lattice with void space occupied with particles. As mentioned above, three different particles were investigated in this study for both effective thermal conductivity and forced convection experiments with particle as working fluid (discussed later). Each case above was tested at three different heat flux values imposed on the top skin (Fig. 1) to ensure that the reported k_{eff} is independent of the thermal boundary condition and is only a function of the porosity, solid-phase thermal conductivity, and unit cell topology (same across all three samples in this study). Figure 6 shows the k_{eff} for packed bed of particles. It was observed that the packed bed k_{eff}

was similar for all particles with diameters varying between 266-966 μm with an averaged value of ~ 0.4 W/mK. Note that these experiments were conducted at nearly room temperature (20-50℃) and the radiation effects were negligble.

The 2nd set of experiments were conducted on Octet lattice with void space occupied by air. Figure 7 shows the k_{eff} values for the three lattice samples with actual porosities varying from 0.712 to 0.867. The k_{eff} was found to be a strong function of porosity where the averaged values over different heat flux levels varied as 2.87, 2.43, and 1.36 W/mK for lattice actual porosities of 0.712, 0.772, and 0.867, respectively. In this case as well, the k_{eff} was independent of the applied heat flux.

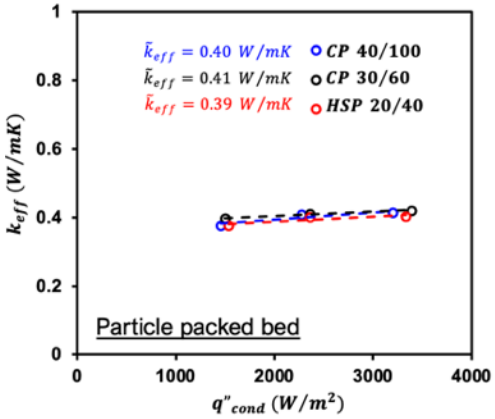

Fig. 6 Effective thermal conductivity of packed bed of particles

The 3rd set of k_{eff} experiments were conducted on lattices with void space being occupied by the particles with diameters varying from 266 – 966 μm (Fig. 8).

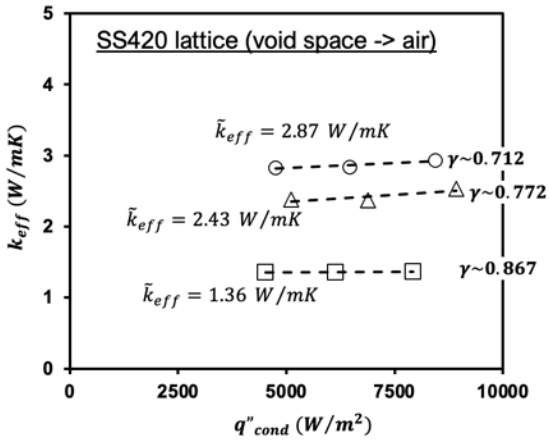

Fig. 7 Effective thermal conductivity of Octet lattice (void space occupied by air)

For the lowest lattice porosity, the particles had some impact on the k_{eff} where the largest particle size had the lowest k_{eff}. This is attributed to the packing efficiency of particles in the void space of Octet unit cells. The two higher particle sizes had near similar k_{eff} values indicating that their packing effiencies were nearly the same when packed in the Octet void space. Note that CP 40/100 and CP 30/60 particle diameters are significantly smaller than that of HSP 20/40. At the two higher values of actual lattice porosities, the particle diameters did not have much impact on the overall k_{eff} values and they performed nearly identical to each other. There was clear decreasing trend in the k_{eff} value with increasing lattice porosity, which is again consistent for the case when void space was occupied by air, indicating that particles don't alter the dominant impact of fibers and their intrinsic thermal conductivity values, even though particles are nearly 16 times more thermally conductive than air.

Figure 9 presents the relative enhancement in k_{eff} values for the lattice when particles packed in void space in reference to a packed bed of particles. This enhancement in k_{eff} is one mode which implicitly affects the overall thermal transport between the hot and cold sides. The relative enhancmene in k_{eff} ($\eta_{k_{eff}}$) was highest for the two lower particle diameters compared to the largest diameter (HSP 20/40). Further, a rapid decline in $\eta_{k_{eff}}$ was observed with increasing lattice porosity. CP 30/60 particles appeared to strike a good balance with similar enhancement levels as CP 40/100, whereas lattice porosity of 0.8 is a balance when porosity is concerned. When dealing with particle flows through obstructions, in this case Octet unit cell array, it is imperative to keep the particles' flowability into account, since low lattice porosities may result in particle clogging. Hence, in order to strike an overall balance between lattice porosity and particle diameters, a combination of CP 30/60 with lattice porosity of 0.8 is a good choice.

3.2 Forced convection with air as "working fluid"

This sub-section presents steady-state experimental results on local convective heat transfer coefficient offered by Octet unit cells when packed between two parallel plates (integrally manufactured) with air as the convective agent. This configuration is typical of the shell-and-plate type configurations currently being investigated at the Sandia National Laboratories. The 2nd hypothesis for enhancing the overall convective heat transfer coefficient between hot and cold sides of a falling particle type heat exchanger is through enhancing the particle-to-solid wall/fiber interstitial heat transfer coefficient. The air-based experiments were conducted for averaged flow velocities randing from 3.4 to 8.4 m/s for all three lattice topologies. For a given lattice porosity, a developing heat transfer trend was observed closer to the inlet where the heat transfer in the first row of Octet unit cells was significantly higher compared to the ones immediately downstream. The heat transfer achieved near periodicity (i.e. it repeats iself) after 5th row and stays nearly constant for another 10 rows (with slightly increasing trend).

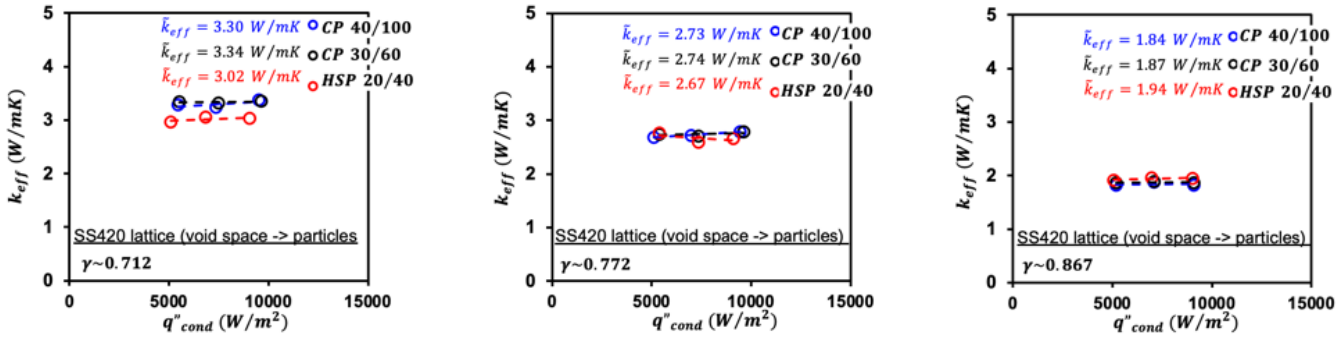

Fig. 8 Effective thermal conductivity of Octet lattice (void space occupied by particles)

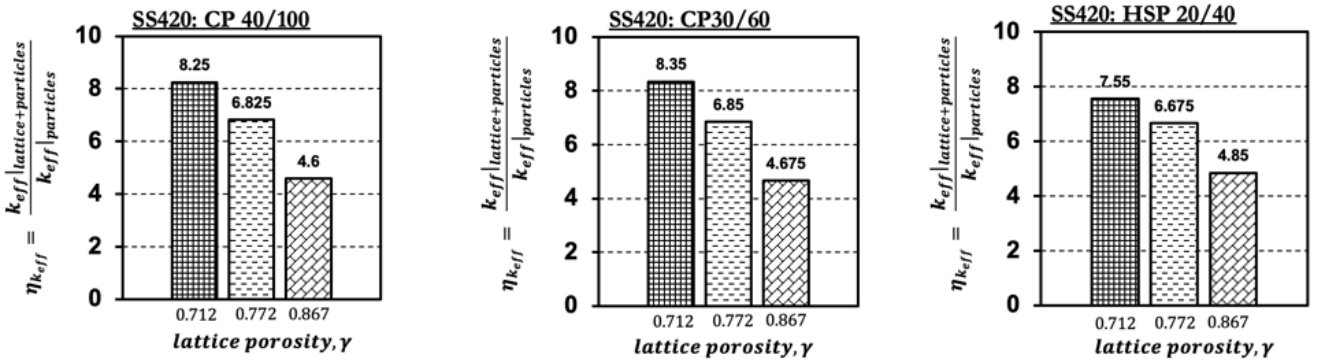

Fig. 9 Effective thermal conductivity enhancement ($\eta_{k_{eff}}$) of Octet lattice packed with particles in reference to packed bed of particles

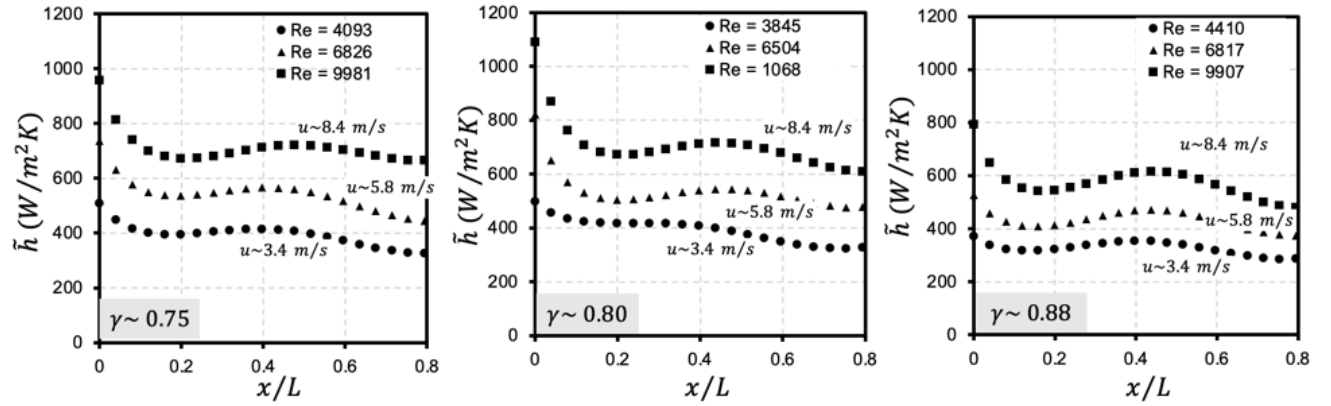

Fig. 10 Local convective heat transfer coefficient variation with lattice porosity

Towards the exit, the heat transfer showed slight reduction. The two lower lattice porosities 0.75 and 0.8 had nearly similar heat transfer levels for all three velocity conditions, whereas the highest porosity 0.88 panel had distinctly lower heat transfer levels compared to the other two higher ones. This is again attributed to multiple factors which include lower effective thermal conductivity and smaller fiber diameters offering less venues of stagnation-type heat transfer enhancement as compared to the larger diameter configurations. The aim of these experiments was to quantify both the developing and developed behavior of the Octet cell rows in terms of the heat transfer enhancement.

It should be noted that in the case of plane channel, the heat transfer coefficient variation with streamwise location would have showed a steep decline and a constant value convergence in very short distance from the inlet. The Octet lattices offer significant enhancement in heat transfer, both in the developing and developed region, with sustained enhanced heat transfer levels. Hence, the employment of Octet unit cells between two parallel plates is hypothesized to provide significant

enhancement in overall heat transfer coefficient of the heat exchanger.

3.3 Forced convection with particle as "working fluid"

An underlying hypothesis behind the testing program with air as working fluid, was that the heat transfer enhancements realized with air would also translate when replaced with particles as working fluid. There are two competing mechanisms here, firstly, packed bed of particles is ~16 times more thermally conductive than air, but this study was conducted when particles were stationary. In a moving packed bed, it is difficuly to isolate the effective thermal conductivity from the overall heat transfer coefficient which is in turn an implicit function of effective thermal conductivity and the intersititial heat transfer coefficient. Second, it is expected that the voidage will be higher when particles are moving in a packed bed configuration when compared to the stationary packed particles, and this voidage is expected to be further higher when the packed bed of particles move in presence of complex arrangement of fibers, in this case Octet. So although the hypothesis was the heat transfer gains observed with air are going to be retained in case of particles, it still needed to be tested. To this end, a novel quasi-steady state heat transfer technique was used to determine time-dependent local convective heat tansfer coefficient by carrying out measurements for over 30 minutes during the slow heat ramp-up phase of the experiment as described in Section 2.3.

Figure 11 shows the transient heat transfer measured at five locations in the streamwise direction for three types of particle flows through Octet panel of porosity 0.88. Only the highest porosity of panel was chosen since we wanted to study the particle diameter effect on the local heat transfer behavior of Octet panels and that the two lower porosities of the Octet panel (0.75 and 0.8) did not support unobstructred free flow of particles of all the diameters. In a follow-up study, we will also present the results for 0.8 porosity lattice with CP 30/60 particles, since that case is considered to strike a good balance between heat transfer performance and particle handling capabilities. For the smallest particle diameter (266 μm), the streamwise location closest to the hopper showed a fluctuating trend with a certain time period. The heat transfer levels at 5% of the streamwise length was nearly two times higher or more compared to the subsequent downstream measurement locations. Further, it is noted that the heat transfer coefficients are nearly constant over a period of 30 minutes which falls under the "quasi-steady" state regime of the transient experiment. For the intermediate particle diameter case (CP 30/60), the fluctuations in transient heat transfer coefficients were not observed and the time evolution of the same showed a nearly constant trend. The heat transfer rates were lower compared to the smallest particle diameter case (CP 40/100). This can be attributed to two factors: a) due to the smaller particle size, the particle flow speeds will be higher for CP 40/100 compared to CP 30/60, b) particle-to-particle, particle-to-gas, particle-to-fiber/endwall interactions will be more frequent for the smallest diameter case.

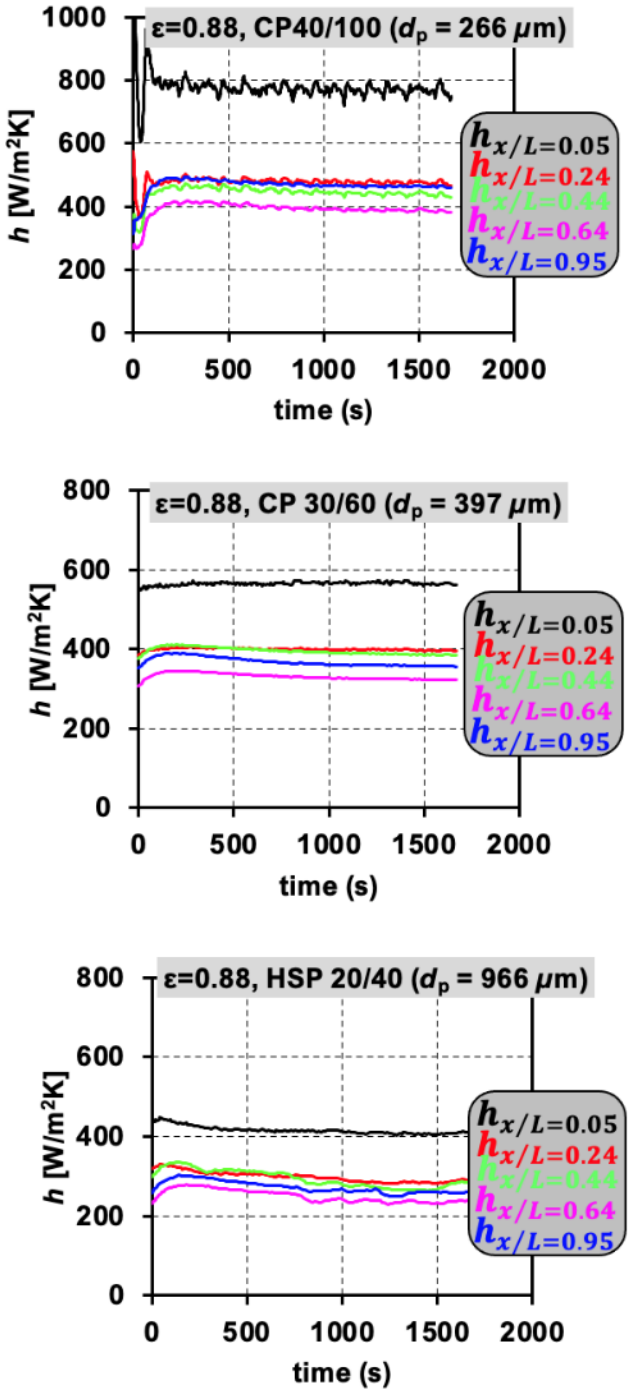

Fig. 11 Transient convective heat transfer coefficient at five different locations in the streamwise direction for three particle types (Octet panel porosity of 0.88)

The 2nd point should be further explore to Discrete Element Modeling (DEM) of particle flows through Octet lattices. For the largest diameter case (HSP 20/40), the heat transfer levels were further lower, thus supporting above two reasonings,

while the temporal evolution exhibited some large time period fluctucations. However, the quasi-steady-state approach worked well for this particle case as well, as the heat transfer levels were nearly constant over the test duration.

Figure 12 shows the time-averaged convective heat transfer coefficient for particle flows through Octet lattice of 0,88 porosity. Figure 11 demonstrates that such a time-averaging is justified as the heat transfer coefficient was found to be time-independent in the quasi-steady state duration. A rapidly decreasing trend in heat transfer rates was observed with increasing streamwise distance, which is a typical trend in developing thermal and fluid flow scenarios.

A near-perioidic heat transfer regime was also observed at the 0.44 and 0.64 x/L locations, which can be considered as representative of the heat transfer coefficient to be expected for particle flows through long panels featuring Octet-shaped unit cells. A slightly increasing trend in heat transfer was observed towards the exit and this trend is attributed to the exit effects. The decrease in the heat transfer rates was only marginal in the x/L -> (0.44,64) regime for particle diameters 266 and 397 μm, however, a significant drop in heat transfer was observed for the largest particle diameter case.

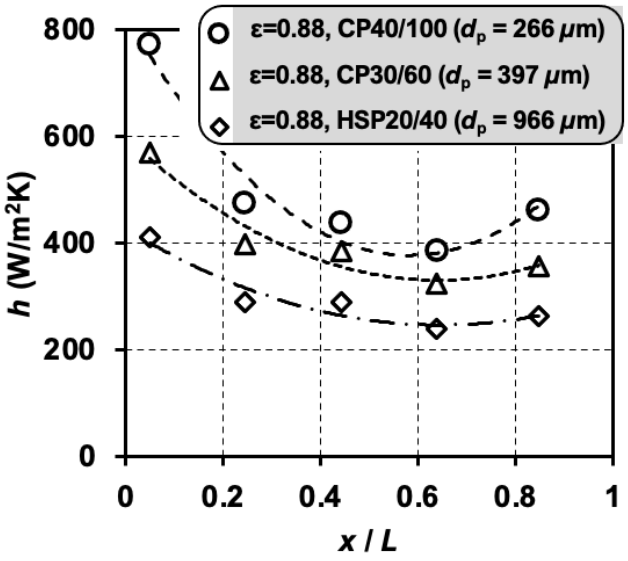

Fig. 12 Time-averaged convective heat transfer coefficient variation with streamwise location (Octet panel porosity of 0.88)

This behavior also justifies the choice of 397 μm as a balance between the two extremes, while it also presents better handling capabilities without significantly compromising on the heat transfer capabilities.

CONCLUSIONS

A comprehensive experimental program has been undertaken to evaluate the heat transfer performance of Octet-shaped unit cells for their capabiltiies to provide convective heat transfer enhancement with air and particles as the carrier fluids. To this end, three different experimental facilities were developed to measure the effective thermal conductivity, convective heat transfer coefficient with airas working fluid, and convective heat transfer coefficient with particles as working fluid. The following major conclusions have been drawn from this work:

(a) Packing the void space of Octet lattice with particles results in thermal conductivity enhancements ranging from 4 to 8 times that of the packed bed of particles. Maximum benefits were observed for the lowest lattice porosity.
(b) Convective heat transfer coefficients for lattice porosities of 0.75 and 0.8 with air as working fluid were nearly similar with values ranging between 650-700 W/m^{2}K for air flow velocity of 8.4 m/s.
(c) For particle flow through Octet lattice of porosity 0.88, the convective heat transfer coefficient was ~400 W/m^{2}K for CP 40/100 and CP 30/60 particles. A near-constant heat transfer was observed after 40% of the streamwise length.

ACKNOWLEDGMENTS

This material is based upon work supported by the U.S. Department of Energy's Office of Energy Efficiency and Renewable Energy (EERE) under the Solar Energy Technologies Office Award Number DE-EE0009377. This report was prepared as an account of work sponsored by an agency of the United States Government. Neither the United States Government nor any agency thereof, nor any of their employees, makes any warranty, express or implied, or assumes any legal liability or responsibility for the accuracy, completeness, or usefulness of any information, apparatus, product, or process disclosed, or represents that its use would not infringe privately owned rights. Reference herein to any specific commercial product, process, or service by trade name, trademark, manufacturer, or otherwise does not necessarily constitute or imply its endorsement, recommendation, or favoring by the United States Government or any agency thereof. The views and opinions of authors expressed herein do not necessarily state or reflect those of the United States Government or any agency thereof.

REFERENCES

[1] Brun, Klaus, Peter Friedman, and Richard Dennis, eds. Fundamentals and applications of supercritical carbon dioxide (sCO2) based power cycles. Woodhead publishing, 2017.
[2] Gautam, Abhishek, and R. P. Saini. "A review on technical, applications and economic aspect of packed bed solar thermal

energy storage system." Journal of Energy Storage 27 (2020): 101046.
[3] Kuravi, Sarada, et al. "Thermal energy storage technologies and systems for concentrating solar power plants." Progress in Energy and Combustion Science 39.4 (2013): 285-319.\
[4] Alaqel, Shaker, et al. "Experimental investigation of the performance of a shell-and-tube particle-to-air heat exchanger." Solar Energy 204 (2020): 561-568.
[5] Ho, Clifford K. "A review of high-temperature particle receivers for concentrating solar power." Applied Thermal Engineering 109 (2016): 958-969.
[6] Ho, Clifford K., and Brian D. Iverson. "Review of high-temperature central receiver designs for concentrating solar power." Renewable and Sustainable Energy Reviews 29 (2014): 835-846.
[7] Ho, Clifford K., et al. "Evaluation of alternative designs for a high temperature particle-to-sCO2 heat exchanger." Journal of Solar Energy Engineering 141.2 (2019).
[8] Reznicek, Evan P., et al. "Simulation of the supercritical CO2 recompression Brayton power cycle with a high-temperature regenerator." Energy Conversion and Management 229 (2021): 113678.
[9] Ho, Clifford K., et al. "Evaluation of alternative designs for a high temperature particle-to-sCO2 heat exchanger." Journal of Solar Energy Engineering 141.2 (2019).
[10] Tan, Zhoutuo, et al. "Numerical investigation of heat transfer for elliptical tube in granular flow using DEM." Energy Procedia 158 (2019): 5504-5509.
[11] Qiu, Lin, et al. "Study on heat transfer of process intensification in moving bed reactor based on the discrete element method." Chemical Engineering and Processing-Process Intensification 151 (2020): 107915.
[12] Baumann, Torsten, and Stefan Zunft. "Development and performance assessment of a moving bed heat exchanger for solar central receiver power plants." Energy Procedia 69 (2015): 748-757.
[13] Jiang, Binfan, et al. "Effective waste heat recovery from industrial high-temperature granules: A Moving Bed Indirect Heat Exchanger with embedded agitation." Energy 208 (2020): 118346.
[14] Albrecht, Kevin J., et al. "Testing and model validation of a prototype moving packed-bed particle-to-sCO2 heat exchanger." AIP Conference Proceedings. Vol. 2303. No. 1. AIP Publishing LLC, 2020.
[15] Albrecht, Kevin J., and Clifford K. Ho. "Design and operating considerations for a shell-and-plate, moving packed-bed, particle-to-sCO2 heat exchanger." Solar Energy 178 (2019): 331-340.
[16] Fang, Wenchao, et al. "Predicting heat transfer coefficient of a shell-and-plate, moving packed-bed particle-to-sCO2 heat exchanger for concentrating solar power." Energy 217 (2021): 119389.
[17] Albrecht, Kevin J., et al. "Development and Testing of a 20 kW Moving Packed-Bed Particle-To-sCO2 Heat Exchanger and Test Facility." Energy Sustainability. Vol. 84881. American Society of Mechanical Engineers, 2021.
[18] Kaur, Inderjot, and Prashant Singh. "Flow and thermal transport through unit cell topologies of cubic and octahedron families." International Journal of Heat and Mass Transfer 158 (2020): 119784.